International Journal of Climatology

The 18.6-year nodal tidal cycle and the bi-decadal precipitation oscillation over the plains to the east of subtropical Andes, South America.

Journal:	*International Journal of Climatology*
Manuscript ID:	JOC-13-0020.R1
Wiley - Manuscript type:	Research Article
Date Submitted by the Author:	20-May-2013
Complete List of Authors:	Agosta, Eduardo; Pontificia Universidad Católica Argentina, PEPACG . CONICET
Keywords:	bidecadal precipitation variability, 18.6-year nodal cycle, climate variability, southern South America, precipitation, grape yield

The 18.6-year nodal tidal cycle and the bi-decadal precipitation oscillation over the plains to the east of subtropical Andes, South America

Eduardo Andres Agosta

Pontificia Universidad Católica Argentina, Ciencia y Técnica (UCA CyT)

Consejo Nacional de Investigaciones Científicas y Técnicas (CONICET)

Short title: **Nodal tidal cycle influence on precipitation in southern South America**

Corresponding author's address:

Alicia Moreau de Justo 1600, Suite 301, Buenos Aires, C1107AFF, Argentina

Telephone +54 11 4349 0200 ext. 7091, fax: ext. 7090.

e-mail: eduardo.agosta@conicet.gov.ar

Sponsors: This research was supported by CONICET's PIPs 112-2009-0100439 and 114-201001-00250 (2011-2013); ANCyT's PICTs 2007-00438 and 2007-01888 (ICES/IDAC); and UBA's UBACYT X-016. Expressed gratitude is given to the Carmelite Order for all their help.

Abstract

The present work shows statistical evidence for lunar nodal cycle influence on the low-frequency summer-rainfall variability over the plains to the east of subtropical Andes, in South America, through long-term SST variations induced by the nodal amplitude of diurnal tides over southwestern South Atlantic (SWSA). In years of strong (weak) diurnal tides, tide-induced diapycnical mixing makes SST cooler (warmer) together with low (high) air pressures in the surroundings of the Malvinas/Falklands Islands in the SWSA, possibly through mean tropospheric baroclinicity variations. Since the low-level tropospheric circulation anomalies directly affect the interannual summer-rainfall variability, such an influence can be extended to the bidecadal variability present in the summer rainfall owing to the nodal modulation effect observed in the tropospheric circulation. The identification of the nodal periodicity in the summer-rainfall variability is statistically robust.

Key words: bidecadal precipitation variability, 18.6-year nodal cycle, climate variability, southern South America, precipitation, grape yield

1. Introduction

Bi-decadal climate variability may have substantial socio-economic impacts on specific regions where the oscillation is significantly observed. The bi-decadal oscillation is known to be prominent on the climate of the North Pacific at inter-decadal timescale (Cook et al., 1997; Minobe et al., 2002; Osafune and Yasuda, 2006; McKinnell and Crawford, 2007; Yasuda, 2009). In the broad (10-100 yr) timescale of interdecadal climate variability, stochastic forcing appears to be a major forcing mechanism, however, what determines the time scale of a specific interdecadal variability remains unclear (Liu, 2012). One candidate for the bi-decadal climate variation in certain regions of the globe is the 18.6-year nodal cycle (Currie, 1984; Yasuda et al., 2006). The nodal cycle is caused by the moon's orbital fluctuation around the earth. The moon's orbital surface is inclined by about 23.4° to the earth equatorial surface and this inclination fluctuates from 18.3° to 28.6° with a period of 18.613 years (Loder and Garret, 1978). The lunar nodal cycle exerts a long-term modulation of lunar diurnal and semidiurnal oceanic tides which eventually can affect climate (Loder and Garret, 1978; Ray, 2007). The mechanism proposed for the tide-climate connection is simple (Loder and Garret, 1978): Especially in summer, when the water column is being warmed and stratified by insolation, tidal currents control the vertical oceanic mixing which may affect sea surface temperatures (SSTs) and then other climatic variables, such as sea level pressure (SLP). The mechanism is more effective over prominent topographic features, such as around islands, coasts and large continental shelves, as well as where strong horizontal SST gradients are present (Loder and Garret, 1978; Tanaka et al., 2012). Likewise Ray (2007) has shown that the tide-climate connection is more likely to be detected in diurnal tidal regimes rather than semidiurnal owing to the relatively weak nodal modulation of the latter. In addition to offering a comprehensive review of the possible connection between tides and the decadal climate variability, the author also has discussed the caveats and the misleading paths of the issue.

Particularly for the North Pacific basin, Yasuda et al. (2006) showed using a simplified layered ocean model that the 18.6-yr. nodal tidal cycle (hereafter 18NTC) could play a role as a basic forcing for the bi-decadal ocean and climate variations. In periods of strong tides, tide-induced diapycnical mixing makes surface salinity and density higher and the upper-layer shallower along the western boundary current. Hence the coastal depth adjustment by baroclinic Kelvin wave enhances the thermohaline circulation, the upper-layer poleward western boundary current and the associated heat transport. The mechanism thus could explain the warmer SST in the Kuroshivo-Oyashio Extension regions, where positive feedback with the Aleutian Low might amplify the bidecadal variations (Yasuda et al., 2006). Furthermore, tree-rings reconstructed Pacific Decadal Oscillation (PDO) time series show statistically significant periodicities of 18.6-year period (Yasuda, 2009). More recently, Tanaka et al. (2012) have shown, by using a state-of-the-art numerical coupled climate model, that the spatial distribution of diapycnical diffusivity together with its 18NTC estimated from a global tide model can reproduce the SST and the SLP variability patterns in the North Pacific that are in part reminiscence of the well-known PDO mode (Mantua et al., 1997).

Most of the evidence linking the 18NTC and bi-decadal climate variations is from the North Pacific basin and continental surrounding areas, probably because instrumental, historical and paleoclimatic data are more available in the Northern Hemisphere than in the Southern Hemisphere, and not because the relationship is absent there. Particularly in southern South America a robust bi-decadal climate signal is found for the summer

(Oct-Mar) rainfall over the plains of central-west Argentina, to the east of subtropical Andes (Compagnucci et al., 2002). The region is currently known by the Spanish name “Nuevo Cuyo” (NC, Fig. 1). The NC region exhibits arid-to-semiarid conditions under the rain shadow of the high subtropical Andes Mountains. Such a climate favors grape production under irrigation to such an extent that this is the main grape-growing region in Argentina (Agosta et al. 2012). The relationship between the NC summer precipitation variability and the tropospheric circulation at interannual scale has been intensively examined by Agosta and Compagnucci (2008, 2012). The bi-decadal oscillation in the NC summer precipitation results in alternating wet and dry spells, lasting approximately 9 years each, from the early 1900s until the early 1970s (Compagnucci et al. 2002). From 1973 to the early 2000s a wet spell is observed perturbing the bidecadal oscillation towards lower frequencies. As a consequence of the extended wet spell, the regionally averaged precipitation undergoes an increase of about 24% in the last decades (Agosta and Compagnucci, 2012). The precipitation increment is in agreement with changes in the frequency of the principal modes associated to the synoptic tropospheric circulation in southern South America resulting from the 1976/77 climate transition (Agosta and Compagnucci, 2008). Furthermore, Agosta and Compagnucci (2012) have found that the climate transition relates to SH tropospheric teleconnections changes affecting the year-to-year variation of summer rainfall in the NC region.

Agosta et al. (2012) studied the relationship between the regional climate and the annual grape yield in the Mendoza Province that is located in the core of NC. The period of study is 1979-2010 corresponding to the extended wet period. The authors have shown that wet (dry) summers are counterproductive (productive) for the grape yields within the net balance all through a decade. Hence, understanding the nature of the bi-decadal variability present in the regional precipitation and its response to the tropospheric teleconnection changes owing to the 1976/77 climate transition can shed more light on the long-term regional socio-economic impacts helping local decision-makers.

Therefore, the aim of the present research is two-folded: in one hand it will examine in more detail the bi-decadal component that is present in the NC summer precipitation variability relating to the climate transition of 1976/77. In the other hand it will fill the information gap existing in the Southern Hemisphere by showing regional evidence for the potential link between bidecadal summer rainfall variation in the NC region, SLP and SST in the southwestern South Atlantic (SWSA) oceanic region and the 18NTC.

2. Data and Methods

2.1 Instrumental data

The low-frequency summer precipitation variability in NC is examined by estimating the interannual summer rainfall index (SRI) in the period 1901-2011 (number of observations N=112) from instrumental precipitation data at 11 meteorological stations (see Fig. 1 and Table 1) provided by the 'Servicio Meteorológico Nacional' (the Argentine Weather Service), following Agosta and Compagnucci (2012). The year of the index corresponds to the end of the summer extending from October to March. The baseline used for the anomalies is 1961–1990 for which positive (negative) values of SRI denote percentage deviation from normal of summer spatial averages.

Instrumental time series of monthly SLP and surface air temperature (SAT) data at two meteorological stations in the Malvinas/Falklands Islands are obtained from the Global Historical Climate Network Monthly version 2 (GHCN-M2, available at http://www.ncdc.noaa.gov/ghcnm/v2.php). One station is Cape Pembroke (51°.70S, 57°.70W, 16m above sea level) with records in the periods 1895-1930 and 1940-1947; and the other is Stanley (51°.70S, 57°.90W, 51m above sea level) with records in the period from 1922 to 1982. Unfortunately, SLP records at the Stanley station are discontinued between 1983 and 1991 and those records observed after 1992 are inconsistent with the previous observations, for this reason it is not possible to extend the historical time series until present time (Woodworth et al., 2005). The normalized 18NTC is determined for the period 1896-2011 according to Yndestad (2006), for which positive values indicate stronger diurnal tide modulation.

2.2 Atmospheric and oceanic gridded data

In addition to instrumental records, additional gridded data are used for historical analysis of low level atmospheric circulation. The second version of the Hadley Center monthly SLP reconstructions (HadSLP2) is provided by the UK Met Office on a 5° latitude x 5° longitude global grid (available at http://www.metoffice.gov.uk/hadobs/). The 20th Century Reanalysis V2 data (20CR) are provided by the NOAA/OAR/ESRL PSD on a 2° latitude x 2° longitude global grid (available at http://www.esrl.noaa.gov/psd/). Likewise historical SST time series are examined using the 2° latitude-and-longitude simple grid average SST Release 2 dataset, provided until 2007 by the International Comprehensive Ocean-Atmosphere Data Set (ICOADS, available at http://icoads.noaa.gov/data.icoads.html). In order to characterize the climatology of SST and low-tropospheric baroclinicity in the SWSA oceanic region during the satellite information period, it is used of NOAA Optimal Interpolation (OI) monthly reconstructions version 2 on a 1° latitude and 1° longitude global grid (available at http://www.esrl.noaa.gov/psd/data/) together with atmospheric data from ERA-interim (ERI) reanalysis, provided on a 0.79° latitude-and-longitude gridded resolution by the European Centre for Medium-Range Weather Forecasts (ECMWF, available at http://www.ecmwf.int).

2.3 Time series analysis

Spectral analysis of historical time series is determined by using the Multi-Taper Method (MTM) according to Ghil et al. (2002) and is implemented by using of the SSA-MTM software program freely available at http://www.atmos.ucla.edu (Vautard et al. 1992). Time series are band-pass filtered using a Fast Fourier Transform (FFT) algorithm in 'Matlab' code in order to isolate the bidecadal component (Jackson 1996). The FFT method reconstitutes desired amplitudes of a time series using an interval of frequencies at around the 18.6-year periodicity (the nodal cycle). The frequencies included in the interval, and their number, vary according to the length of the series. Linear relationships between variables are determined by means of the Pearson's first moment correlation, using a two-tail test with degree of freedom d.f. = N-2, where N is the sample size. The degrees of freedom in the bidecadal component time series is corrected as d.f. = N/18.6yr (Yasuda 2009).

2.4. The tide-climate connection

As mentioned in the introduction, the seminal paper of Loder and Garrett (1978) suggests a possible mechanism through oceanic tides for the association between the 18.6-year period oscillation of the lunar orbital inclination and climate. Variations in oceanic tides directly modulate vertical diapycnical mixing that brings colder water to the surface, thereby periodically cooling surface water and the overlying atmosphere. According to Ray (2007) a true tide-climate connection because of the nodal cycle must be found in regions of intense diurnal tides. In such regions the primary fingerprint would be a general cooling effect from enhanced tidal mixing during periods in which the moon's declination maximizes respect to the equator plane (every 9.3 years, half a nodal cycle). The effect can extend into the atmosphere by means of a direct mechanism, in which a negative SST anomaly locally cools the lower atmosphere to induce a downward flow accompanied by a positive SLP anomaly, and vice versa. An example of this seems to be identified in the inner Okhotsk Sea (Tanaka et al., 2012). The effect can further extend into the atmosphere by means of an indirect mechanism, to such an extent that it influences bidecadal variability in basin-scale climate (Loder and Garrett 1978; Yasuda et al. 2006; McKinnell and Crawford 2007). In the indirect mechanism, positive feedbacks between mid-latitude air-sea interactions (through changes in mean baroclinicity, storm tracks position, SST fronts, etc.) can amplify the SST effects on the atmosphere and locally shift further the phase of anomalies. Additionally appropriate atmospheric teleconnections could conceivably extend the effect over larger regions. An example of indirect mechanism is found in the North Pacific basin: Seemingly, during strong tidal mixing, a large positive SST anomaly extends into the Kuril Straits and the Okhotsk Sea and along the Kuroshio–Oyashio Extension region where tidal mixing is very weak, surrounded by negative SST anomaly in the eastern and northern North Pacific as well as in the equatorial Pacific. In turn, the Aleutian low is weakened and shifted northwestward during strong tidal mixing. The obtained anomalous SST and SLP patterns are similar to those associated with the negative phase of the PDO (Yasuda et al. 2006; Yasuda 2009; Tanaka et al. 2012).

3. Results

3.1. Summer rainfall variability and its bidecadal component

The low-frequency variability of the interannual SRI time series is shown in Fig. 2a. The overall behavior shows a significant positive linear trend (correlation of 0.19, significant at α=0.05) and relevant interannual variability (vertical bars). Since only the stationary component of low-frequency processes within the instrumental period are to be analyzed, the linearly detrended SRI time series is considered for further analysis. An extended wet period is evident after the early 1970s. According to Agosta and Compagnucci (2012), this wet period is a consequence of the climate transition of 1976/77 that perturbs interdecadal oscillations. Accordingly, in the period 1901-1977 the MTM power spectrum for the SRI time series shows low-frequency peaks in the bandwidth of about 14.2-19.0 years (α≤0.10), and the maximum power is at about 18.0 years, significant at α< 0.045 (Fig. 2b). When the information of the full period (1901-2011) is added, the bidecadal peak is reached in the bandwidth of about 18.3-25.0 years (α≤0.10) and the maximum power is at about 22.7 years, significant at α< 0.038 (Fig. 2c). Note that he 18.6-year periodicity associated with the 18NTC noticeably appears as a spectral line, significant at α< 0.057 for the period 1901-1977 and at α< 0.029 for the full period. There is also presence of two peaks at about 4-4.5 years and 2.1 years with a 95% confidence for both periods, and another peak at about 15.8 years in the period 1901-2011, significant at α≤0.10. The bi-decadal modulation of the SRI time series reconstituted by the FFT band-pass filter centered at about 18.6 years is shown by the smoothed curve in Fig. 2a. The smoothed time series explains about 21% of the interannual variance of summer rainfall in the decades before the 1980s. Henceforth the explained variance is about 5%. Consequently, from both the spectral analysis and the filtering reconstitution is evident the presence of a bidecadal component in the SRI variability, closely related with the 18NTC, that is strong until mid-1970s and weaker in the last decades likely due to the natural climate shift observed since then.

3.2. Summer rainfall variability, sea level pressure over southwestern South Atlantic and the nodal tidal cycle

According to Agosta and Compagnucci (2012) the 1976/77 climate shift produced changes in the tropospheric teleconnections affecting the SRI interannual variability. Before 1976/77 the tropospheric circulation that influences the SRI interannual variability is related with quasi-stationary waves that propagate from the southern tropical Indian and western Pacific basins; while afterwards it is related with zonally elongated anomalies that propagate poleward from central equatorial Pacific, associated with El Niño-like warmer conditions. In either of the two detected types of teleconnection, low-level tropospheric circulation anomalies located at mid-latitudes in SWSA play a major role in transporting wet air masses from the ocean to the interior of the continent (Agosta and Compagnucci (2012). The correlation between the detrended SRI time series and SLP field from HadSLP2 for summer is shown in Figure 3a, denoting a large center of action positioned over SWSA. The core of the center of action is near the Malvinas/Falklands Islands (at about 51-52°S, 61-59°W). This result suggests that at interannual scales anomalous anticyclonic (cyclonic) low-level circulation in the SWSA propitiates wet (dry) summer conditions in the NC region.

Note that this link between the summer rainfall variability in the NC region and the low-level tropospheric circulation over SWSA has been previously identified by Agosta and Compagnucci (2008) using Principal Component Analysis applied on daily reanalysis data and by Agosta and Compagnucci (2012) using composite techniques on zonally asymmetric anomalies of monthly tropospheric circulation.

At this point the question is whether the field of air mass over the SWSA also presents the bidecadal modulation. This requires identifying appropriate SLP long time series in this region. Instrumental time series of monthly SLP data are accessible in the islands of Malvinas/Falklands at two close stations, one in Cape Pembroke and the other in Stanley. Because of proximity, the summer average SLP records at the Stanley can be linearly interpolated into the past by using the records from the Cape Pembroke station. The linear fitting between both time series offers a correlation of 0.97. Hence the summer SLP data interpolated at the Stanley station can be used for analysis in the extended period 1896-1982 (N=87). The Stanley SLP time series for summer is compared with the SLP time series at the nearest gridded point drawn from both the HadSLP2 and the 20CR datasets. The 20CR SLP dataset is used for comparison. Note that the correlation between Stanley SLP and HadSLP2 SLP time series at the nearest gridded point yields a robust value of 0.70 in the period 1896-1982, being significantly different from zero at $\alpha<0.01$. Moreover in the same period the correlation between Stanley SLP and the 20CR time series at the nearest gridded point is moderate ($r=0.46$, significant at $\alpha<0.01$). Hence the historical representation of the SLP in the SWSA obtained by the HadSLP2 reconstructed dataset yields more robust results. In turn, in the period 1901-1982, the correlation between the detrended SRI and the Stanley SLP is 0.66 (significant at $\alpha<0.01$), while the correlation for detrended SRI and HadSLP2 SLP time series at the nearest gridded point is lower, 0.40, significant at $\alpha<0.01$. The latter means that any analysis of the interannual (and probably of lower frequency) variability between the SRI time series and SLP time series in the SWSA area will yield more realistic results using historical station records than reconstructed ones. Hereinafter, the SLP time series of Stanley and HadSLP2 dataset will be used to examine the bidecadal variability potentially present in the low-level atmospheric circulation.

The multitaper power spectral analysis applied to these SLP time series yields some spectral peaks in the bidecadal band, albeit not significant. The wavelet power spectrum (Torrence and Compo, 1998) shows that the bidecadal spectral lines are significant at a 90% confidence level, tested against white noise (figures not shown). Figure 3b illustrates the bidecadal smoothed time series of the SRI, Stanley SLP and HadSLP2 SLP at the nearest gridded point for summer, together with the normalized 18NTC. It is clear that the bidecadal component present in the Stanley SLP time series and the HadSLP2 SLP time series is pertinent since it explains 12% and 9% of the variance for each interannual time series, respectively. In turn, the maximum bidecadal amplitude for Stanley SLP is about 1mb, being larger than for HadSLP2 SLP at the nearest gridded point, which is 0.5mb.

Figure 3b further shows that the bidecadal modulation of the subtropical summer rainfall (bars) is highly synchronized with the nodal cycle (thin line). The in-phase relationship is persistent throughout the record-length. The correlation between the bidecadal components of SRI and 18NTC yields a very strong negative maximum value without lag, r=-0.97, significant at $\alpha<0.001$ (d.f. = 6). The bidecadal modulation of the SLP time series (dotted line) is mostly in-phase related with the 18NTC (thin line) during the whole period, with a positive lag of one-to-two years in some epochs. The correlation between them, however, is maximum without lag, r=-0.88, significant at $\alpha<0.02$ (d.f. = 4.7). The lagged phase relationship with the nodal cycle is more prominent for the HadSLP2 SLP series (square line) at the nearest gridded point during the last decades. An overall two-year lag inverse correlation of r=-0.75, significant at $\alpha<0.05$ (d.f. = 6), is observed between HadSLP2 SLP series and 18NTC series. The result suggests that the inverse phase relationship with the nodal cycle is more robust for the Stanley SLP time series. The HadSLP2 reconstruction appears to be slightly less appropriate to capture the bidecadal component present in the air mass field over the SWSA, as was pointed out further above.

3.3. Nodal modulation of surface air temperature and sea surface temperature over southwestern South Atlantic

Any 18.6-year modulation induced by the moon on oceanic tidal currents should be detected by changes in oceanic circulations linked to the tidal mixing (diapycnical mixing) that modify the heat transport and ultimately impact on the amplitudes of SST. However, historical in-situ SST records are scarce and intermittent in the SWSA. A local proxy of SST is the SAT station data recorded in Malvinas/Falkland Islands. Hence monthly SAT time series at the Stanley station and the Cape Pembroke station are used to support the previous findings. The SAT time series at both stations have similar discontinuity problems as those for the SLP data (see previous section). Unlike SLP, there is no possibility of linear fitting between the temperature data from Cape Pembroke and Stanley since their correlation is 0.57 for summer in the overlapping period. The bidecadal components in the summer SAT time series are identified after band pass filtering. Figure 4a shows the bidecadal smoothed SAT time series at Cape

Pembroke (dotted line) and Stanley (dashed line) together with the 18NTC (thin line). The overall bidecadal variation in the Cape Pembroke SAT time series is weak with an amplitude of 0.15°C and an explained variance of hardly 2%. Instead, for the Stanley station, the bidecadal SAT modulation has amplitude of 0.7°C and explains 16% of the interannual variance. In general the SAT time series are inverse related with the nodal cycle and drift gradually over time. Nodal modulations of climate variables are not expected to remain fixed over long time periods. According to Ray (2007) small changes in phase are to be anticipated since tidal mixing can vary as stratification and other ocean parameters vary. Furthermore, the phase relationship between the SAT time series at Cape Pembroke and the SAT time series at Stanley is one-to-two years lagged in the period of overlap (1923-1947), probably because of relative different response to the tidal-induced mixing. In consequence, it is possible to state that the SAT timeseries fluctuate synchronically with the SLP time series in the surroundings of the Malvinas/Falklands Islands. This suggests that higher (lower) surface pressures are accompanied by warmer (cooler) SSTs throughout a nodal modulation.

The result is further confirmed using ICOADS SST data. In order to compare the gridded SSTs with the previous station SAT time series, summer SSTs are averaged on an area around the Malvinas/Falklands Islands (53-51°S, 59-57°W) in the SWSA. Figure 4b illustrates the bidecadal smoothed time series of summer SSTs of the spatial average for the period 1896-2007 together with the 18NTC. The bidecadal modulation accounts for 8% of the interannual variance of summer SST and has overall amplitude of 0.5°C. As expected, an apparent inverse and phase-locked relationship with the nodal cycle is persistent all through the 20th century. The inverse relationship indicates that the nodal modulation acting on the SST variation over SWSA is essentially through the diurnal tides. The strongest negative correlation is obtained with lag zero and yields a value of r = -0.77 in the period 1896-2007, significant at $\alpha<0.05$ (d.f. = 6). This result is consistent with those shown in Fig.1b of Tanaka et al. (2012). Using a global tide model the authors demonstrate that the tidal energy dissipation induced by the 18.6-year oscillation amplitude is in phase with diurnal tides in the region that extends from the western border of the Patagonia shelf in the SWSA poleward, and in the surroundings of the Antarctic Peninsula in the Weddell Sea. Hence their model result together with our observational finding further suggest that nodal tide-induced SST anomalies can extend along the western boundary current, in the limit of the Patagonian shelf.

3.4. A mechanism linking the low-frequency SST and SLP fluctuations in SWSA

The previous results show that during the course of a nodal cycle strong (weak) diurnal tides occur with cool (warm) SST anomalies and low (high) SLP anomalies in the surroundings of the Malvinas/Falklands Islands, and presumably over a larger area in the SWSA. It is easy to verify through correlation between the ERI summer SLP time series, obtained as an spatial average in the vicinity of the Malvinas/Falkland Islands, and the OI summer SST field that such a relationship between SLP and SST is likewise supported at interannual scale in the period 1982-2012 and that it extends over the Patagonian shelf (figures not shown). Note further that this oceanic region is characterized by strong horizontal SST gradients (Fig. 5a) and enhanced lower tropospheric baroclinicity (Fig. 5b), because of the confluence of the warm-Brazil/cold-Malvinas Currents (Matano et al., 2010). Several authors suggest the importance of mid-latitude oceanic fronts in shaping the tropospheric circulation and its variability

(Nakamura and Shimpo, 2004; Minobe et al., 2008; Nakamura et al., 2008; Deremble et al. 2012). Variations in the intensity and position of a strong SST front produce anomalous sensible heat and moisture fluxes that alter the mean baroclinicity. The latter can shift the position of the mid-latitude storm tracks, which can be noted in the seasonal average as tropospheric circulation anomalies, such as SLP anomalies.

How this mechanism of mid-latitude oceanic front/atmosphere interaction is active in the SWSA remains to be investigated and it is beyond the scope of the current research. Nonetheless, there is some evidence that supports it. Tokinaga et al. (2005) have shown that the SST front along 49°S to the northeast of the Malvinas Falkland Islands induces surface wind changes both at monthly and interannual scales through the Coriolis Effect acting on the wind acceleration/deceleration. They further suggest that SST-induced surface wind variations over the Brazil–Malvinas Confluence could modify the lower-tropospheric baroclinicity and the storm track position. Therefore it is suggested here an indirect mechanism that could provide the observed regional tide-climate linking: Long-term SST variations, that are induced by the nodal amplitude of diurnal tides and transported northward by the Malvinas Current, can modify the intensity of the SST front that possibly alter the lower tropospheric baroclinicity. In turn changes in baroclinicity can generate SLP fluctuations in the SWSA that are ultimately related with the summer rainfall variation in the NC region all through a nodal cycle.

4. Concluding remarks

The present work shows, for first time, statistical evidence for lunar nodal cycle influence on low-frequency variability of summer-rainfall in the plains to the east of subtropical Andes in South America. The link can be established through SST modulation that is induced by the nodal amplitude of diurnal tides over SWSA. In years of strong (weak) diurnal tides, nodal tide-induced diapycnical mixing makes SST cooler (warmer) that are accompanied by low (high) SLP anomalies affecting the mid-latitudes low-level tropospheric circulation. The SST variations would presumably affect the lower tropospheric baroclinicity in the surroundings of the Malvinas/Falklands Islands in the SWSA, which in turn would induce shifts of mid-latitude storm track. Note that long-term changes in the mid-latitude cyclonic activity at synoptic scale are determinant of summer rainfall variations in the NC region (Agosta and Compagnucci 2008). Furthermore, as previously shown in Agosta and Compagnucci (2012), summer tropospheric circulation anomalies located over SWSA directly affect the interannual variability of summer rainfall. The current research further shows that such an influence can be extended into the bidecadal variability observed in the summer rainfall owing to the nodal modulation effect. The identification of the nodal periodicity in the NC summer rainfall variability is statistically robust. Although the 1976/77 climate shift has mitigated the bidecadal component of the summer rainfall variability until the early 2000s, the nodal cycle has always been present. Hence the nodal cycle information could improve the interdecadal predictability of the mean conditions of the summer rainfall and of those socio-economic variables that are sensitive to precipitation such as grape yield in the Mendoza Province.

References

Agosta, E.A. and Compagnucci, R. H. (2008), The 1976/77 austral summer climate transition effects on the atmospheric circulation and climate in southern South America. J. Climate, 21, 4365–4383.

Agosta, E.A. and Compagnucci, R. H. (2012), Central-West Argentina Summer Precipitation Variability and Atmospheric Teleconnections. J. Climate, 25, 1657–1677.

Agosta, E.A., Canziani, P.O. and Cavagnaro, M.A. (2012), Regional Climate Variability Impacts on the Annual Grape Yield in Mendoza, Argentina. J. Appl. Meteor. Climatol., 51, 993–1009.

Compagnucci, R. H., Agosta, E. A. and Vargas, M. W. (2002), Climatic change and quasi-oscillations in central-west Argentina summer precipitation: Main features and coherent behavior with southern African region. Climate Dyn., 18, 421–435.

Cook, E. R., D. M. Meko, and C. W. Stockton (1997), A new assessment of possible solar and lunar forcing of bidecadal drought rhythm in the western United States, J. Clim., 10, 1343– 1356.

Currie, R. G. (1984), Evidence for 18.6-year lunar nodal drought in western North America during the past millennium. Journal of Geophysical Research: Atmosphere, 89, 1295-1308. DOI: 10.1029/JD089iD01p01295.

Deremble, B., Lapeyre, G, and Ghil, M. (2012): Atmospheric Dynamics Triggered by an Oceanic SST Front in a Moist Quasigeostrophic Model. Journal of Atmospheric Sciences, 69, 1617-1632. DOI: 10.1175/JAS-D-11-0288.1

Ghil , M, M. R. Allen, M. D. Dettinger, K. Ide, D. Kondrashov, M. E. Mann, A. W. Robertson, A. Saunders, Y. Tian, F. Varadi, and P. Yiou (2002), Advanced spectral methods for climatic time series, Rev. f Geoph., 40, 1, 1-41.

Haigh, I. D., M. Eliot, and C. Pattiaratchi (2011), Global influences of the 18.61 year nodal cycle and 8.85 year cycle of lunar perigee on high tidal levels, J. Geophys. Res., 116, C06025, doi: 10.1029/2010JC006645.

Hoskins, B. J., and P. J. Valdes (1990): On the existence of stormtracks. J. Atmos. Sci., 47, 1854–1864.

Jackson, L. B., (1996): Digital filters and signal processing: with MATLAB exercises. Kluwer Academic Publishers, 502 pp.

Liu, Zhengyu, (2012): Dynamics of Interdecadal Climate Variability: A Historical Perspective. J. Climate, 25, 1963–1995.

Loder, J. W., and C. Garrett (1978), The 18.6-year cycle of sea surface temperature in shallow seas due to variation in tidal mixing, J. Geophys. Res., 83, 1967– 1970.

McKinnell, S. M., and W. R. Crawford (2007), The 18.6-year lunar nodal cycle and surface temperature variability in the northeast Pacific, J. Geophys. Res., 112, C02002, doi: 10.1029/2006JC003671.

Mantua, N. J., S. R. Hare, Y. Zhang, J. M. Wallace, and R. C. Francis (1997), A Pacific interdecadal climate oscillation with impacts on salmon production. Bull. Amer. Meteor. Soc., 78, 1069–1079.

Matano, R.P., E.D. Palma and A.R. Piola (2010), The influence of the Brazil and Malvinas Currents on the southwestern Atlantic shelf circulation. Ocean Sci. Discuss., 7, 837–871. www.ocean-sci-discuss.net/7/837/2010/

Minobe, S., T. Manabe, and A. Shouji (2002), Maximal wavelet filter and its application to bidecadal oscillation over the Northern Hemisphere through the twentieth century, J. Clim., 15, 1064–1075.

Minobe, S., A. Kuwano-Yoshida, N. Komori, S.-P. Xie, and R. J. Small (2008), Influence of the Gulf Stream on the troposphere. Nature, 452, 206–209, doi:10.1038/nature06690.

Nakamura, H., and A. Shimpo (2004), Seasonal variations in the Southern Hemisphere storm tracks and jet streams as revealed in a reanalysis dataset. J. Climate, 17, 1828–1844.

Nakamura, H., A. Goto, W. Ohfuchi, and S.-P. Xie, (2008), On the importance of midlatitude oceanic frontal zones for the mean state and dominant variability in the tropospheric circulation. Geophys. Res. Lett., 35, L15709, doi:10.1029/2008GL034010.

Osafune, S. and I. Yasuda (2006), Bidecadal variability in the intermediate waters of the northwestern subarctic Pacific and the Okhotsk Sea in relation to 18.6-year period nodal tidal cycle, J. Geophys. Res., 111, C05007, doi:10.1029/2005JC003277.

Ray, R. D. (2007), Decadal climate variability: Is there a tidal connection?, J. Clim., 20, 3542–3560.

Tanaka, Yuki, Ichiro Yasuda, Hiroyasu Hasumi, Hiroaki Tatebe, Satoshi Osafune (2012), Effects of the 18.6-yr Modulation of Tidal Mixing on the North Pacific Bidecadal Climate Variability in a Coupled Climate Model. J. Climate, 25, 7625–7642.

Tokinaga, Hiroki and Y. Tanimoto (2005), SST-Induced Surface Wind Variations over the Brazil–Malvinas Confluence: Satellite and In Situ Observations, J. Clim, 18, 3470-3482.

Torrence, C., and G. P. Compo (1998), A practical guide to wavelet analysis. Bull. Amer. Meteor. Soc., 79, 61–78.

Vautard, R., P. Yiou, and M. Ghil (1992), Singular-spectrum analysis. :a toolkit for short, noisy chaotic signals. Physica D, 58, 95-126.

Woodworth, P. L., D. T. Pugh, M. P. Meredith, and D. L. Blackman (2005), Sea level changes at Port Stanley, Falkland Islands, J. Geophys. Res., 110, C06013, doi:10.1029/2004JC002648.

Yasuda, I., S. Osafune, and H. Tatebe (2006), Possible explanation linking 18.6-year period nodal tidal cycle with bi-decadal variations of ocean and climate in the North Pacific, Geophys. Res. Lett., 33, L08606, doi:10.1029/2005GL025237.

Yasuda, I. (2009): The 18.6-year period moon-tidal cycle in Pacific Decadal Oscillation reconstructed from tree-rings in western North America, Geophys. Res. Lett.,36, L05605, doi: 10.1029/2008/GL036880.

Yndestad, H. (2006): The influence of the lunar nodal cycle on Arctic climate. ICES Journal of Marine Science, 63: 401e420. doi:10.1016/j.icesjms.2005.07.015

Table 1: Meteorological stations used to devise summer rainfall index (SRI) in the 'Nuevo Cuyo' region at approximately 28º-37ºS and 65º-70ºW (see also Fig. 1). LRJ: La Rioja Observatorio. SNJ: San Juan Observatorio. CHE: Chepes. MZA: Mendoza Observatorio. SNL: San Luis Observatorio. VMC: Villa Mercedes/Reynolds. SCR: San Carlos. RMC: Rama Caída/San Rafael. COL: Colonia Alvear. MAL: Malargüe. VTR: Victorica.

Station name	height (m)	Latitude (ºS)	Longitude (ºW)	Record
LRJ	516	29.42	66.87	1904-2011
SNJ	634	31.32	68.57	1900-2011
CHE	658	31.33	66.60	1930-1990
MZA	769	32.88	68.82	1900-2011
SNL	734	33.03	66.32	1905-2011
VMC	514	33.68	65.48	1900-2011
SCR	940	33.77	69.01	1938-1979
RMC	713	34.67	68.40	1927-2011
COL	465	35.00	67.69	1935-1979
MAL	1425	35.50	69.58	1953-2011
VTR	312	36.23	65.43	1905-2011

Figure Captions:

Figure 1: Map showing the region of study in South America: The plains to the east of subtropical Andes known as "Nuevo Cuyo" (NC, between 37-28°S, 69°-66°W), the southwestern South Atlantic (SWSA) oceanic region and the Malvinas/Falklands (M/F) Islands (~51°S, 59°W). The acronyms LRJ, CHE, SNJ, MZA, SNL, VMC, SCL, RMC, MAL, COL, VTR are for the meteorological stations within NC, (see Table 1).

Figure 2: a) The summer rainfall index (SRI) time series, expressed as percentage deviation from normal (bars), the corresponding smoothed curve (dotted line) around the nodal cycle is obtained by FFT reconstitution using the frequencies 1/15.9, 1/18.5 and 1/22.2 in cycles yr^{-1}, and its linear trend curve (LT, straight line). The linear equation and its explained variance (R^2) are given. b) The multitaper power spectrum (three tapers) of annual SRI (thick curve) in the period 1901-1977 with 50% (median, thin curve), 90% (short dash) and 95% (long dash) significant levels for a red noise process. The x-axis shows periodicity in years as reference. c) Idem panel b), but for the annual SRI time series in the period 1901-2011.

Figure 3: a) Correlation between detrended annual SRI and detrended summer-average HadSLP2 in the period 1901-2011. The shaded areas show the significance levels as shown by the lateral bar. b) The smoothed curves around the nodal cycle, obtained by a FFT reconstitution using the frequencies 1/15.9, 1/18.5 and 1/22.2 in cycles yr^{-1} for SRI (bars), using the frequencies 1/14.5, 1/17.4, and 1/21.8 in cycles yr^{-1} for SLP at Stanley (dotted line) and using the frequencies 1/14.6, 1/16.7, 1/19.5 and 1/22.2 in cycles yr^{-1} for SLP at the nearest gridded point from HadSLP2 dataset (square line), together with the normalized nodal cycle (18NTC, thin line).

Figure 4: a) Smoothed curves around the nodal cycle for surface air temperature (SAT) time series of summer average, obtained by FFT reconstitution using the frequencies 1/13.0, 1/17.3 and 1/26.0 in cycles yr^{-1} for the time series at Cape Pembroke (dotted line) and using the frequencies 1/15.0 and 1/20.0 in cycles yr^{-1} at Stanley (triangle line) together with the normalized nodal cycle (18NTC, thin line). b) Idem panel a) but for sea surface temperature (SST) from ICOADs, averaged in the area 51-53°S, 59-57°W (dashed line) using the FFT frequencies 1/14.0, 1/16.0, 1/18.7 and 1/22.4 in cycles yr^{-1}, and the normalized nodal cycle (18NTC, thin line).

Figure 5: a) OI SST climatology for summer (Oct-Mar) in the period 1982-2012. Units are in °C. b) lower-tropospheric mean baroclinicity for summer in the period 1980-2012 estimated using the ERI reanalysis data, as measured by the Eddy Growth Rate (EGR) in the layer 1000/700hPa, according to the definition given by Hoskins and Valdes (1990). Units are in s/day.

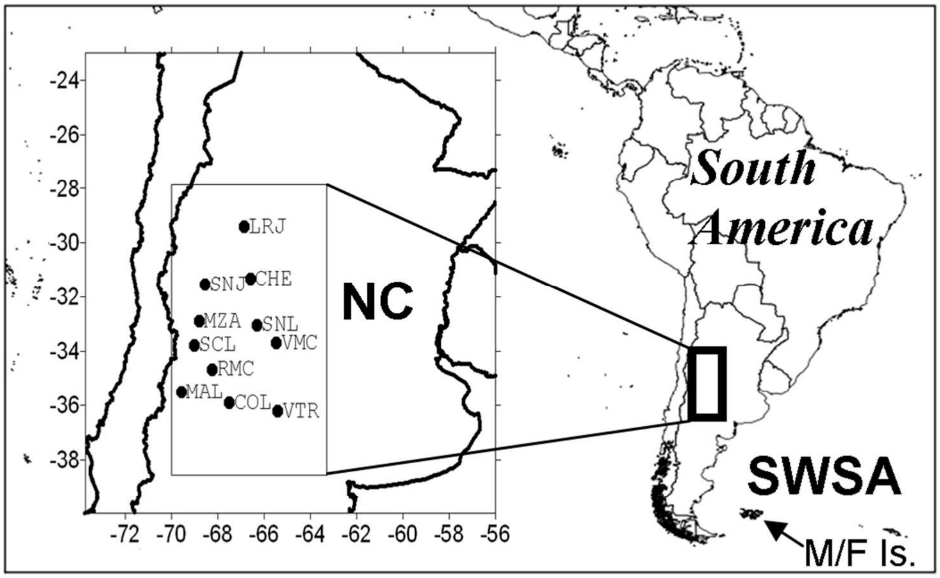

Map showing the region of study in South America: The plains to the east of subtropical Andes known as "Nuevo Cuyo" (NC, between 37-28°S, 69°-66°W), the southwestern South Atlantic (SWSA) oceanic region and the Malvinas/Falklands (M/F) Islands (~51°S, 59°W). The acronyms LRJ, CHE, SNJ, MZA, SNL, VMC, SCL, RMC, MAL, COL, VTR are for the meteorological stations within NC, (see Table 1).
94x59mm (300 x 300 DPI)

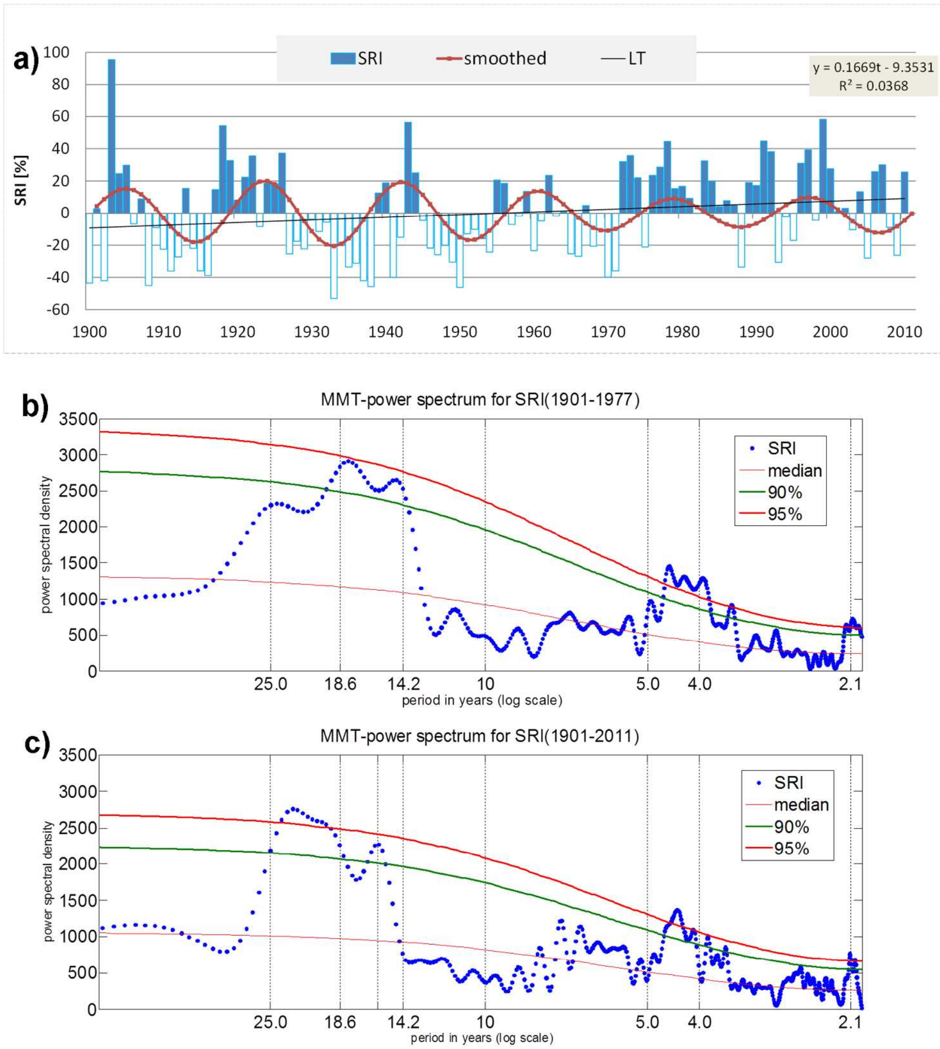

a) The summer rainfall index (SRI) time series, expressed as percentage deviation from normal (bars), the corresponding smoothed curve (dotted line) around the nodal cycle is obtained by FFT reconstitution using the frequencies 1/15.9, 1/18.5 and 1/22.2 in cycles yr−1, and its linear trend curve (LT, straight line). The linear equation and its explained variance (R2) are given. b) The multitaper power spectrum (three tapers) of annual SRI (thick curve) in the period 1901-1977 with 50% (median, thin curve), 90% (short dash) and 95% (long dash) significant levels for a red noise process. The x-axis shows periodicity in years as reference. c) Idem panel b), but for the annual SRI time series in the period 1901-2011.
159x169mm (300 x 300 DPI)

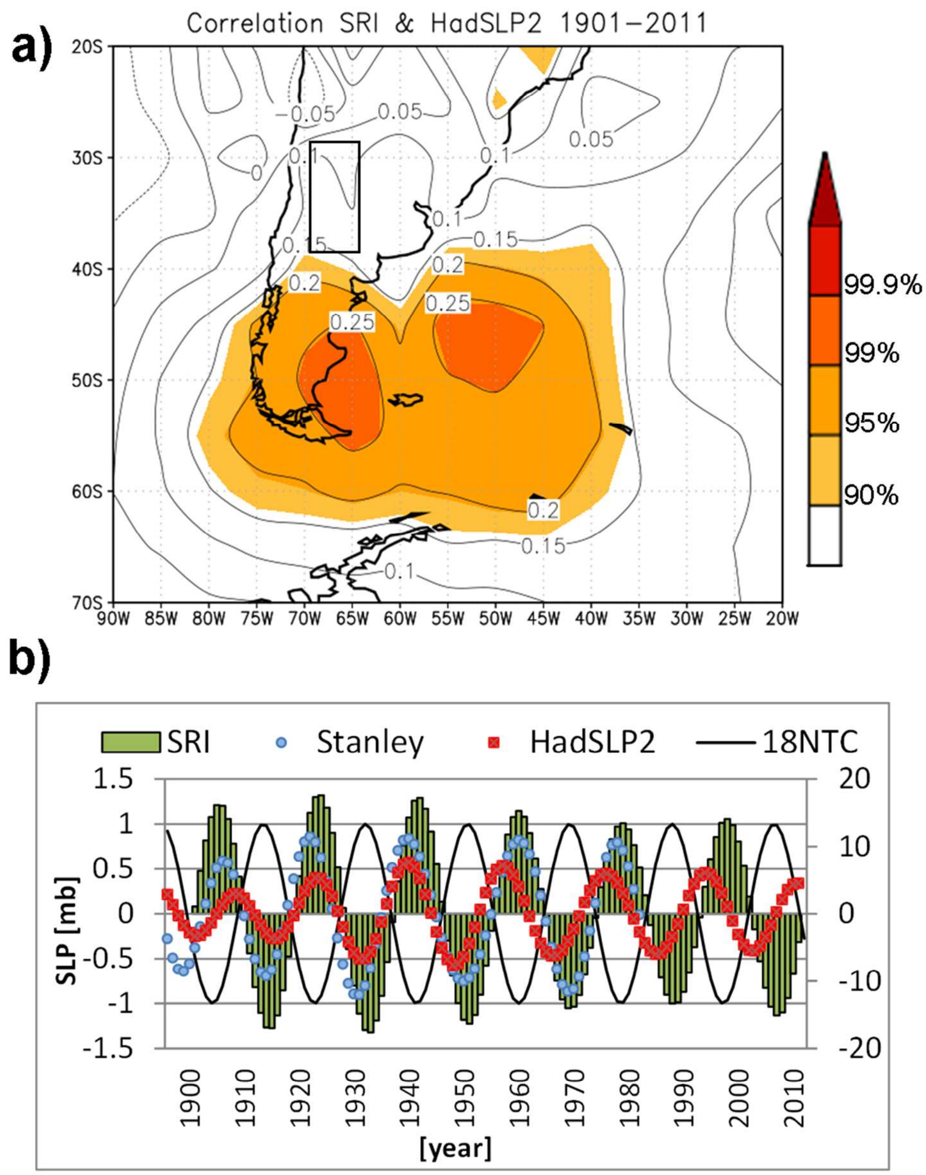

a) Correlation between detrended annual SRI and detrended summer-average HadSLP2 in the period 1901-2011. The shaded areas show the significance levels as shown by the lateral bar. b) The smoothed curves around the nodal cycle, obtained by a FFT reconstitution using the frequencies 1/15.9, 1/18.5 and 1/22.2 in cycles yr−1 for SRI (bars), using the frequencies 1/14.5, 1/17.4, and 1/21.8 in cycles yr−1 for SLP at Stanley (dotted line) and using the frequencies 1/14.6, 1/16.7, 1/19.5 and 1/22.2 in cycles yr−1 for SLP at the nearest gridded point from HadSLP2 dataset (square line), together with the normalized nodal cycle (18NTC, thin line).
94x119mm (300 x 300 DPI)

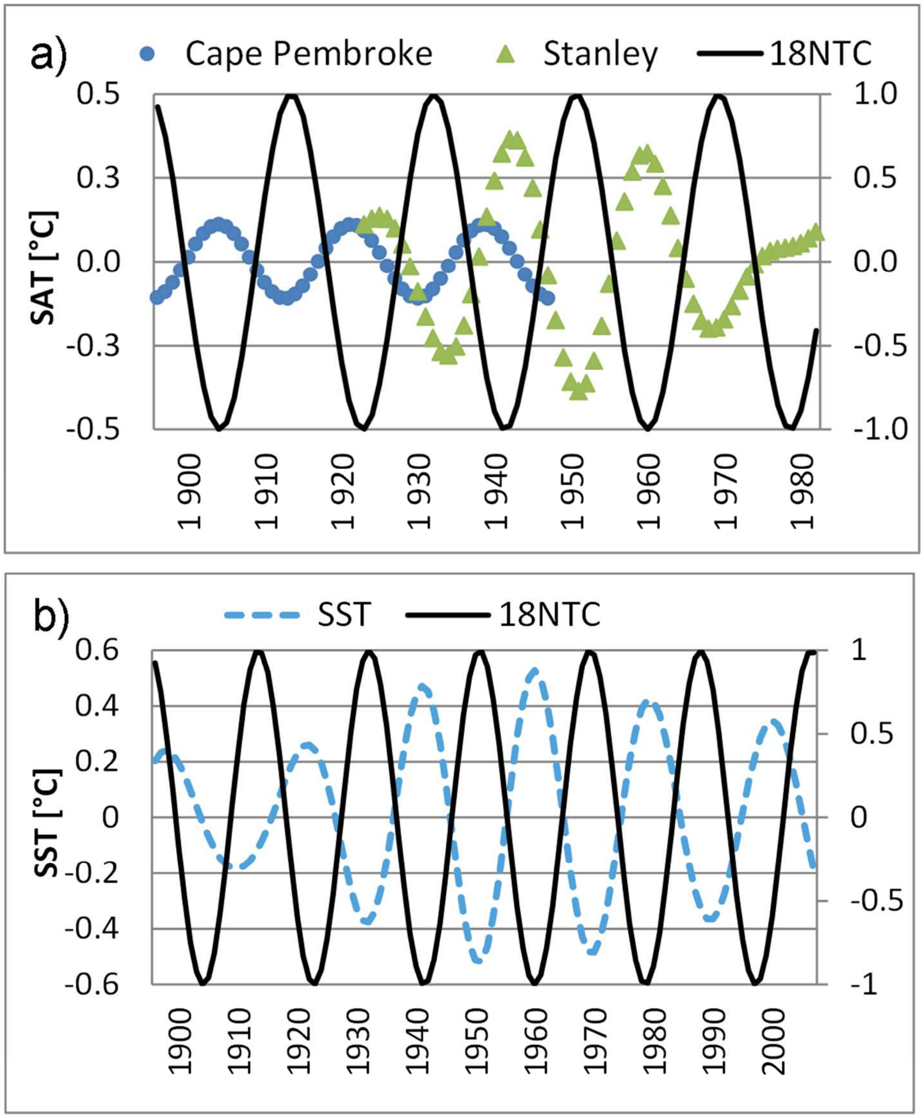

a) Smoothed curves around the nodal cycle for surface air temperature (SAT) time series of summer average, obtained by FFT reconstitution using the frequencies 1/13.0, 1/17.3 and 1/26.0 in cycles yr−1 for the time series at Cape Pembroke (dotted line) and using the frequencies 1/15.0 and 1/20.0 in cycles yr−1 at Stanley (triangle line) together with the normalized nodal cycle (18NTC, thin line). b) Idem panel a) but for sea surface temperature (SST) from ICOADs, averaged in the area 51-53°S, 59-57°W (dashed line) using the FFT frequencies 1/14.0, 1/16.0, 1/18.7 and 1/22.4 in cycles yr−1, and the normalized nodal cycle (18NTC, thin line).
109x129mm (300 x 300 DPI)

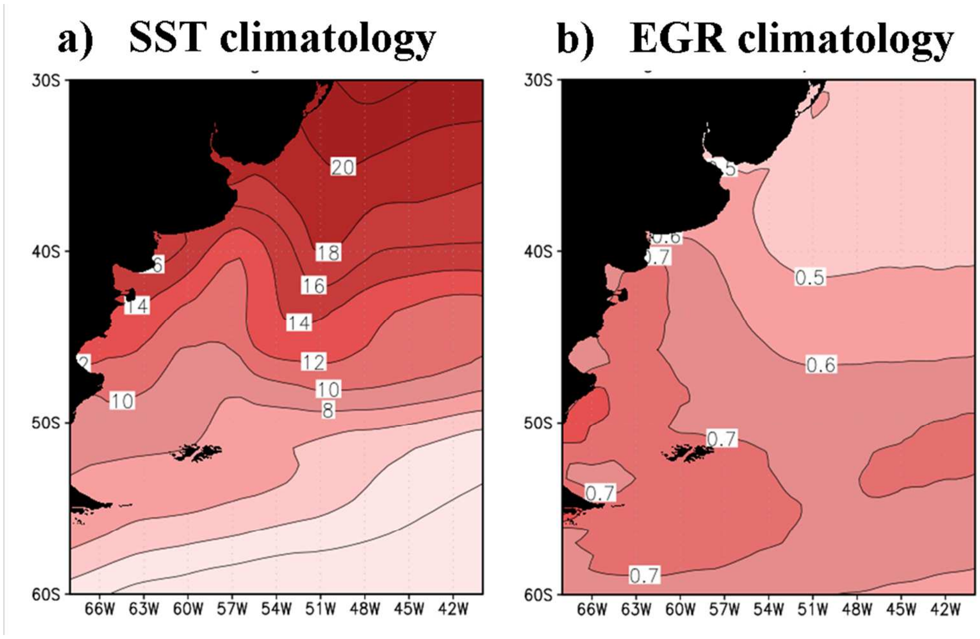

a) OI SST climatology for summer (Oct-Mar) in the period 1982-2012. Units are in °C. b) lower-tropospheric mean baroclinicity for summer in the period 1980-2012 estimated using the ERI reanalysis data, as measured by the Eddy Growth Rate (EGR) in the layer 1000/700hPa, according to the definition given by Hoskins and Valdes (1990). Units are in s/day.
94x59mm (300 x 300 DPI)